Stress and Fold Localization in Thin Elastic Membranes

Luka Pocivavsek, *et al.*

Science **320**, 912 (2008);
DOI: 10.1126/science.1154069

Science (print ISSN 0036-8075; online ISSN 1095-9203) is published weekly, except the last week in December, by the American Association for the Advancement of Science, 1200 New York Avenue NW, Washington, DC 20005.

References and Notes

1. C. L. Carilli, G. B. Taylor, *Annu. Rev. Astron. Astrophys.* **40**, 319 (2002).
2. F. Govoni, L. Feretti, *Int. J. Mod. Phys. D* **13**, 1549 (2004).
3. T. E. Clarke, P. P. Kronberg, H. Böhringer, *Astrophys. J.* **547**, L111 (2001).
4. D. Ryu, H. Kang, P. L. Biermann, *Astron. Astrophys.* **335**, 19 (1998).
5. Y. Xu, P. P. Kronberg, S. Habib, Q. W. Dufton, *Astrophys. J.* **637**, 19 (2006).
6. P. Schuecker, A. Finoguenov, F. Miniati, H. Böhringer, U. G. Briel, *Astron. Astrophys.* **426**, 387 (2004).
7. R. M. Kulsrud, R. Cen, J. P. Ostriker, D. Ryu, *Astrophys. J.* **480**, 481 (1997).
8. D. Nagai, A. Vikhlinin, A. V. Kravtsov, *Astrophys. J.* **655**, 98 (2007).
9. M. Murgia *et al.*, *Astron. Astrophys.* **424**, 429 (2004).
10. C. Vogt, T. Enßlin, *Astron. Astrophys.* **434**, 67 (2005).
11. D. Ryu, H. Kang, E. Hallman, T. W. Jones, *Astrophys. J.* **593**, 599 (2003).
12. C. Pfrommer, V. Springel, T. A. Enßlin, M. Jubelgas, *Mon. Not. R. Astron. Soc.* **367**, 113 (2006).
13. H. Kang, D. Ryu, R. Cen, J. P. Ostriker, *Astrophys. J.* **669**, 729 (2007).
14. K. B. Quest, *J. Geophys. Res.* **93**, 9649 (1988).
15. A. R. Bell, *Mon. Not. R. Astron. Soc.* **182**, 147 (1978).
16. R. D. Blandford, J. P. Ostriker, *Astrophys. J.* **221**, L29 (1978).
17. L. Biermann, *Z. Naturforsch.* **5a**, 65 (1950).
18. E. S. Weibel, *Phys. Rev. Lett.* **2**, 83 (1959).
19. M. V. Medvedev, L. O. Silva, M. Kamionkowski, *Astrophys. J.* **642**, L1 (2006).
20. J. Binney, *Mon. Not. R. Astron. Soc.* **168**, 73 (1974).
21. G. Davies, L. M. Widrow, *Astrophys. J.* **540**, 755 (2000).
22. H. J. Völk, A. M. Atoyan, *Astropart. Phys.* **11**, 73 (1999).
23. P. P. Kronberg, Q. W. Dufton, H. Li, S. A. Colgate, *Astrophys. J.* **560**, 178 (2001).
24. K. Subramanian, K. A. Shukurov, N. E. L. Haugen. *Mon. Not. R. Astron. Soc.* **366**, 1437 (2006).
25. D. Ryu, J. P. Ostriker, H. Kang, R. Cen, *Astrophys. J.* **414**, 1 (1993).
26. R. M. Kulsrud, E. G. Zweibel, *Rep. Prog. Phys.* **71**, 046901 (2008).
27. J. Cho, E. T. Vishniac, *Astrophys. J.* **538**, 217 (2000).
28. B. M. Gaensler, R. Beck, L. Feretti, *N. Astron. Rev.* **48**, 1003 (2004).
29. S. Das, H. Kang, D. Ryu, J. Cho, *Astrophys. J.* **681**, in press (2008).

30. This work was supported by the Korea Foundation for International Cooperation of Science and Technology through grant K20702020016-07E0200-01610 provided by the Ministry of Education, Science and Technology. The work of D.R. was also supported by the Korea Science and Engineering Foundation (KOSEF) through the grant of basic research program R01-2007-000-20196-0. The work of H.K. and S.D. was also supported by KOSEF through the Astrophysical Research Center for the Structure and Evolution of the Cosmos. The work of J.C. was also supported by the Korea Research Foundation, grant KRF-2006-331-C00136, funded by the Korean Government.

Supporting Online Material

www.sciencemag.org/cgi/content/full/320/5878/909/DC1
Materials and Methods
SOM Text
Figs. S1 to S6
References

7 January 2008; accepted 10 April 2008
10.1126/science.1154923

Stress and Fold Localization in Thin Elastic Membranes

Luka Pocivavsek,[1] Robert Dellsy,[2] Andrew Kern,[1] Sebastián Johnson,[3] Binhua Lin,[2] Ka Yee C. Lee,[1] Enrique Cerda[3]*

Thin elastic membranes supported on a much softer elastic solid or a fluid deviate from their flat geometries upon compression. We demonstrate that periodic wrinkling is only one possible solution for such strained membranes. Folds, which involve highly localized curvature, appear whenever the membrane is compressed beyond a third of its initial wrinkle wavelength. Eventually the surface transforms into a symmetry-broken state with flat regions of membrane coexisting with locally folded points, reminiscent of a crumpled, unsupported membrane. We provide general scaling laws for the wrinkled and folded states and proved the transition with numerical and experimental supported membranes. Our work provides insight into the interfacial stability of such diverse systems as biological membranes such as lung surfactant and nanoparticle thin films.

Crumple a piece of paper and a meshwork of highly deformed ridges and perfectly straight planes appear. This focusing behavior is universal for any strongly confined membrane (*1*, *2*). Compress a similar membrane now resting on some substrate like water or a gel, and it responds differently. Its initial response is wrinkling, producing beautiful sinusoidal undulations across the entire surface (*3*–*7*). Yet if the wrinkled surface is laterally compressed even further, a different geometry emerges. The wrinkles disappear everywhere except for a few select locations on the surface that exhibit folds, a geometry similar to the crumpled piece of paper.

[1]Department of Chemistry and James Franck Institute (JFI), University of Chicago, Chicago, IL 60637, USA. [2]Center for Advanced Radiation Sources and JFI, University of Chicago, Chicago, IL 60637, USA. [3]Departamento de Física and Centro para Investigación Interdisciplinaria Avanzada en Ciencias de los Materiales, Universidad de Santiago, Av. Ecuador 3493, Santiago, Chile.

*To whom correspondence should be addressed. E-mail: ecerda@lauca.usach.cl

A variety of real systems can be thought of as elastic membranes resting on softer substrates. Our lungs are lined by a thin membrane, composed of lipids and proteins, that stabilizes them and is often modeled as an elastic sheet on a fluid subphase (*8*–*10*). The membrane's mechanical response via reversible folding is believed to play a key role in normal lung function (*9*). Likewise, thin layers of nanoparticles—which show promise as unique electronic, optical, and magnetic materials (*11*)—have recently been spread at air/water interfaces as a method of controlling their packing structure and to allow ease of deposition onto solid substrates for potential technological use (*12*, *13*). Wrinkling and folding of such layers during deposition could be exploited to create nanopatterned structures.

Several theoretical approaches have been developed to treat particular cases of either wrinkling (*3*, *6*, *7*, *14*–*16*) or folding (*8*, *17*, *18*) in given systems. However, the generality of these instabilities has not been developed, and existing theories treat one state or the other without connecting the two. Here, we explore the evolution of a general elastic interface under lateral compression. We show that wrinkles appear as a first-order linear response of the membrane and can be suppressed by nonlinear effects that give rise to the fold at greater confinement.

A thin (10-μm) sheet of polyester resting on the surface of water is initially flat. Clamping one set of free edges between two movable barriers and compressing by some small amount Δ, the sheet instantaneously forms wrinkles with a wavelength λ (a in Fig. 1A). If the sheet is continually compressed, the wrinkle amplitude grows uniformly across the surface (*19*). Eventually one wrinkle will grow in amplitude, whereas the others decay as seen in b in Fig. 1A. Further confinement leads to the eventual formation of a fold where all of the distortion is focused within a narrow region of the surface (c in Fig. 1A).

Although the wrinkle-to-fold transition in Fig. 1A takes place when the polyester sheet is lying on top of water, a fluid substrate is not necessary for the transition. Figure 1B shows a similar evolution of the surface with the polyester adhered to a soft gel. Smooth wrinkling (a in Fig. 1B) becomes unstable (b in Fig. 1B) and eventually localizes into several folds relaxing the rest of the surface (c in Fig. 1B).

A phenomenologically similar transition can be observed in films three orders of magnitude thinner. At an air/water interface, gold nanoparticles 5 nm in diameter are compressed to form a self-assembled trilayered film that is 15 nm thick. With the use of light microscopy, one can observe the initial periodic wrinkles with $\lambda \sim 10$ μm (a in Fig. 1C). If the compression is stopped, the surface remains wrinkled. However, further confinement leads to the focusing behavior observed in the macroscopic polyester film. Panel b in Fig. 1C shows the beginning of fold formation: The brightness of one wrinkle increases as its amplitude grows, scattering more light. Eventually the two leaflets of the sheet make self-contact, and the fold

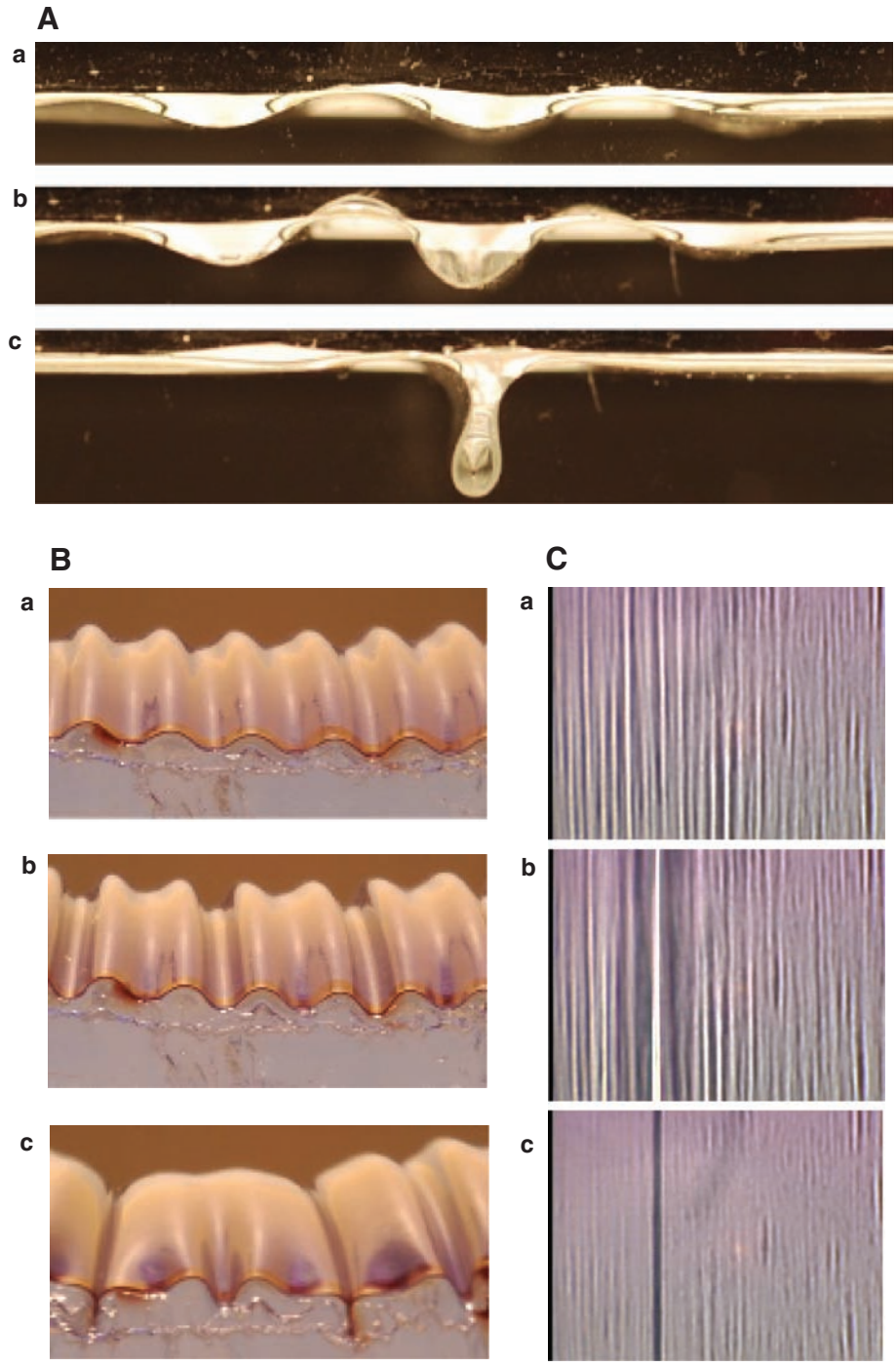

Fig. 1. (**A**) Polyester film on water, (**B**) polyester film on gel substrate [where *K* is much higher than in (A)], and (**C**) trilayer of colloidal gold nanoparticles on water [where *B* is much lower than in (A)] transitioning from an extended wrinkled state, a, to a localized folded state upon further compression, c. Polyester films are 10 μm thick. The nanoparticle layer is 15 nm thick. The macroscopic systems are imaged from the side. The nanoparticles, compressed in a Langmuir trough, are microscopically imaged from above. Panel a in (C) shows a uniform wrinkled surface, with the wrinkle troughs and peaks providing the contrast in brightness. As one wrinkle grows in amplitude, it becomes brighter still [b in (C)]. Upon fold completion [c in (C)], the fold extending underneath the surface is several microns long and far below the focal plane of the surface so scattering is not seen. It appears dark because of its thickness suppressing transmission. As a length scale for each set, one can use the initial wrinkle wavelength: (A), $\lambda \sim 1.6$ cm; (B), $\lambda \sim 3.3$ mm; and (C), $\lambda \sim 10$ μm. The membranes here span three orders of magnitude in thickness and initial wrinkle wavelength. Furthermore, the intermolecular forces holding them together are very different: The polyesters are cross-linked polymers, whereas the gold nanoparticles are simply held together by van der Waals forces (*12*).

(appearing dark) is formed, relaxing the wrinkles to either side. A movie of the process is available as supporting online material (SOM; movie S1) (*20*); also available is a movie showing folding in a model lung surfactant layer (movie S2).

A thin membrane can be bent far more easily than stretched (*1*). As such, thin membranes are often described as inextensible so that their length is preserved upon deformation. In the above experiments, a membrane of length L is compressed by a horizontal distance Δ, so that the total projected length along the horizontal direction is $L - \Delta$. The lack of compression along the plane of the membrane leads to the constraint $L - \Delta = \int_0^L dl \cos\phi$, where the integration and differentiation are in terms of distance along the curve l (arc length). Figure 2A defines ϕ as the angle between the tangent to the curve and the horizontal; the derivative of the angle with respect to arc length ($\dot{\phi}$) gives the curvature.

To understand the observed nonlinear folds, we studied the energy, U, for a thin inextensible elastic sheet. The energy per unit of width is made up of two parts: the elastic bending energy, $U_B = (B/2)\int_0^L dl\,\dot{\phi}^2$, of the film and the potential energy due to the displacement of the substrate underneath, $U_K = (K/2)\int_0^L dl \cos\phi y^2$, where y is the vertical displacement of the surface from the flat state, B is the bending stiffness of the surface, and K is the stiffness of the substrate. In the case of a fluid substrate, Hertz was the first to realize that its weight could act as an effective stiffness; thus, for a fluid $K = \rho g$, where ρ is the fluid density and g is the acceleration due to gravity (*21*).

The shape of the film is obtained by minimization of the total energy $U = U_B + U_K$ with a Lagrangian multiplier to satisfy the inextensibility. To study the weakly confined wrinkled state, we make the linear approximation $\phi \approx \dot{y}$, where $\dot{y}$ is the derivative of the vertical displacement with respect to the arc length. Given a smooth sinusoidal undulation of the surface as seen in the experiments, the bending energy scales as $U_B \approx (B/2)\int_0^L dl\ddot{y}^2 \sim BL(A/\lambda^2)^2$ (where $\ddot{y}$ is the second derivative of the vertical displacement with respect to the arc length), and the potential energy as $U_K \approx (K/2)\int_0^L dl y^2 \sim KLA^2$, where A is the wrinkle amplitude. A balance of these two energies gives the wavelength of the wrinkles as $\lambda \sim (B/K)^{1/4}$ (see fig. S1 and SOM for exact calculation and experimental fitting). Furthermore, the inextensibility in the linear approximation is $\Delta \approx \int_0^L dl\dot{y}^2 \sim L(A/\lambda)^2$. This gives the amplitude as $A \sim \lambda\sqrt{(\Delta/L)}$. The wrinkles are

predicted to grow continuously in amplitude as $\sqrt{\Delta}$, which is in agreement with our observations.

The total energy for a wrinkled state scales as $U \sim (BK)^{1/2}\Delta$ and is distributed across the entire undulating surface. The specific energy U/L has a finite value for a given applied external strain Δ/L independent of the system size. Furthermore, a constant pressure is necessary to confine a film in a wrinkled state $p = \partial_\Delta U \sim (BK)^{1/2}$ (where $\partial_\Delta U$ is the derivative of the energy with respect to the horizontal displacement), independent of the amount of lateral displacement so long as the system size is large (*20*). Thus, the conclusions from the linear analysis are that once a wrinkled surface appears, it is the stationary solution. Further confinement leads to a simple increase in amplitude that gives rise to an increase in energy for the system.

Whereas the above linear analysis explains the wrinkled state, it does not provide insight into the wrinkle-to-fold transition. To examine the transition into the strongly confined state where fold localization begins, we experimentally studied a thin polyester film on water and numerically analyzed the lowest energy solutions to the energy functional defined earlier. The insets in Fig. 3, A and C, show profiles of the physical and numerical sheets as compression is increased. $N = L/\lambda$ and $d = \Delta/\lambda$ are the only dimensionless parameters in the problem (here, N is the number of wrinkles, and d is the dimensionless lateral displacement). A_1 is chosen as the amplitude of the wrinkle that decays and A_0 as the amplitude of the one that grows (Fig. 2A). Both the physical and numerical systems show divergence of the amplitudes from the square root dependence on displacement seen in uniform wrinkles beyond a certain confinement (Fig. 2B). Notably, around $d = \Delta/\lambda \approx 0.3$ (i.e., $\Delta \approx \lambda/3$), A_0 begins to increase linearly, and the buttressing wrinkle amplitude A_1 begins to decay. This is the hallmark of the wrinkle-to-fold transition.

The amplitude data also bring forth an emergent size independence within the folding regime. The wrinkle amplitude derived above depends on strain (Δ/L); however, the fold amplitude depends only on Δ. The fact that the wrinkle-to-fold transition occurs at $d \approx 0.3$ thus gives rise to the increased scatter in the data for $d < 0.3$ and a collapse of the data onto linear curves beyond this critical point (Fig. 2B).

To avoid the finite size effect at low compression, one can look at the ratio of the two amplitudes, A_0/A_1, that acts as an effective order parameter for the transition. For a uniformly wrinkled state, the order parameter should fluctuate around one. However, as confinement increases above a critical point, the order parameter must diverge. Figure 3A shows the overlay of physical (circles) and numerical (solid blue line) data for the order parameter. When $d < 0.3$, both sets lie on the line $A_0/A_1 \approx 1$. As compression is increased beyond this point, there is a seemingly asymptotic divergence.

The theoretical data in Fig. 3A represent an upper bound to the data for the order parameter, which can be explained by considering the final fold shape. In the numerical analysis, up/down as well as S and anti-S folds are seen as final states (Fig. 3B). However, in the polyester experiments, S and anti-S folds eventually relax toward an up/down geometry upon further compression (*22*). In Figs. 2B and 3A, the data are divided between membranes that formed intermediate S and anti-S folds (gray symbols) and those that did not (black symbols). The untwisting is driven by line tension at the polyester/water/air interface, not accounted for in the numerical analysis, and occurs at higher values of d; thus, some physical data are slightly shifted to the right as shown in Fig. 3A (gray circles).

The correspondence between the numerical and physical data attests that the essential physics of the phenomenon is captured in the simulation. Both experiments show that a wrinkled surface should be stable against further confinement by a third of its wavelength ($\lambda/3$), beyond which the surface geometry becomes unstable toward the new localized folded state. The fold eventually collapses as two nonadjacent parts of the surface make self-contact, and confinement approaches the initial wrinkle wavelength.

We now provide a physical interpretation of the transition in the original unscaled variables. For a fold with a maximum curvature at its tip $\dot{\phi}_{max}$, the energy is localized inside a perimeter of $l \sim 1/\dot{\phi}_{max}$ so that the bending energy of the fold scales as $U_B \sim B/l$. The height of the fold is proportional to the applied displacement Δ; hence, the potential energy must scale as $U_K \sim K\,l\Delta^2$. We have not considered the nonlinear effect due to the factor $\cos\phi$ in the potential energy. This term represents the projection of the fold shape along the horizontal direction. Writing the inextensibility constraint as the sum of linear and nonlinear terms, we obtain $\int_0^L dl(1 - \cos\phi) = \Delta$. The potential energy can similarly be divided, $U_K = (K/2)\int_0^L dl y^2 - (K/2)\int_0^L dl(1 - \cos\phi)y^2$. This yields the scaling $U_K \sim Kl\Delta^2 - K\Delta^2\int_0^L dl(1 - \cos\phi) \sim Kl\Delta^2 - K\Delta^3$.

The size of the fold l is obtained by minimizing the total energy $\partial_l (U_B + U_K) = 0$, giving $l \sim (B/K)^{1/2}(1/\Delta)$, which is confirmed by

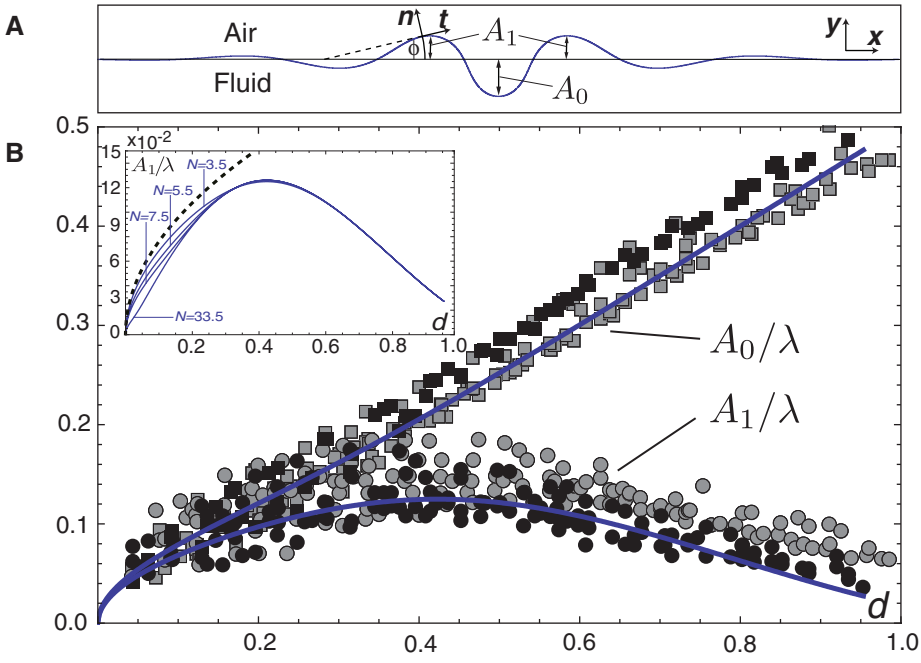

Fig. 2. (**A**) The figure defines A_0 and A_1 and the geometrical parameters describing a confined sheet. The deformation can be described by using a two-dimensional coordinate system. Here t and n are the tangent and normal to the surface, respectively. ϕ gives the position of the tangent with respect to the horizontal direction. (**B**) Experimental results for polyester on water for A_0 (squares) and A_1 (circles). Experimental data were taken for several membrane sizes, including when $N = 3.5$, 4.0, 4.5, 5.0, 5.5, 6.0, 6.5, 7.0, 7.5, and 8.0. Dark solid lines show numerical results for a sheet with $L = 3.5\lambda$. Both the physical polyester and numerical data are made dimensionless. A_1, A_0, and Δ are scaled to λ. (Inset) A_1 versus horizontal displacement for several numerical systems of different sizes (solid blue lines). The dashed line is the theoretical curve $A = [(\sqrt{2})/\pi]\lambda\sqrt{(d/3.5)}$ (*20*) that follows the numerical curve for $N = 3.5$ and $d << 1$. In both numerical and physical cases, the data are more scattered for $d < 0.3$ and then collapse onto more compact (perfectly so in numerical case) curves past this point. This behavior is indicative of the size-dependent behavior in the wrinkling ($d < 0.3$) regime and size-independent behavior in the folding ($d > 0.3$) regime.

our numerical analysis. Thus, the total energy for the folded state in terms of only material constants and displacement is $U \sim (BK)^{1/2}\Delta - K\Delta^3$.

One way to check this energy is to calculate the pressure needed to confine a sheet. From our scaling law, $p = \partial_\Delta U \sim (BK)^{1/2} - K\Delta^2$. In dimensionless form, the pressure can be written as $p/(BK)^{1/2} = a - bd^2$, where a is obtained from the linear analysis [$a \approx 2$, see derivation in (*20*)] and b from fitting the numerics ($b \approx 2.47$) (solid curve in Fig. 3C).

The energies of the wrinkled state and folded state differ only in a term of higher order that is related to the geometry of the localized fold. This term lowers the total energy, which explains why a localized fold is observed for high values of confinement instead of a stationary wrinkled state that extends throughout the surface. Rewriting the scaling in terms of d, the wrinkle and fold energies are within 10% of each other around $d \approx 0.3$. As such, the energy-scaling arguments are in quantitative agreement with the experiments. The fold energy becomes more stable when the sheet is compressed beyond a third of the initial wrinkle wavelength, at which point energy begins to be localized within a narrow part of the surface proportional to l (*23*).

This focusing effect and the wrinkle-to-fold transition should generally occur when the thin membrane and substrate foundation are considerably mismatched in their elastic properties. In the case of a fluid substrate where the fluid has no static elasticity, the transition occurs as described. In the case of soft gels (such as the system in Fig. 1B) where the ratio of the Young's moduli of the membrane (E_m) and substrate (E_s) is ~1000, localization still occurs (c in Fig. 1B) yet is distributed into several folds. Work on very stiff substrates ($E_m/E_s < 100$) has shown the persistence of wrinkles at large confinement with no stress focusing (*24*). We believe the relaxation of wrinkles into multiple folds is linked to the underlying ability of the substrate to stretch and shear. We predict that in the range $1000 > E_m/E_s > 100$, the number of wrinkles relaxing into one fold should decrease, giving rise to a larger number of folds with smaller amplitudes. As the lower limit is reached, surface focusing is suppressed, and the excess membrane length due to compression is accommodated in wrinkles of longer wavelengths and larger amplitudes (*24*).

Many physical examples exist where the mismatch in membrane and substrate elasticity is large. A long-standing problem in supported membranes has been understanding the focused and large-amplitude folds seen in lipid monolayers. More than 50 years ago, Ries and Kimball showed that such monolayers at air/water interfaces develop large-amplitude folds at localized sites on the surface (*25*). Since then, folding has been reported in several other lipid (*10*, *26*) and nanoparticle films (*12*), yet existing theories relying on defects (*8*, *15*, *17*, *18*) fail to account for the universality of how these ultrathin membranes transition from flat structures only nanometers in thickness to folds orders of magnitude larger. We conjecture that the large-amplitude folds in self-assembled layers like lipids and gold nanoparticles initiate via the mechanism explored here. Generally, self-assembled films at air/liquid interfaces should become unstable to wrinkling and folding when they become solidlike and capable of supporting lateral compression (*27*).

Our model also provides an elegant mechanism that accounts for fold size and directionality by simply invoking the film's elastic character and confinement to the interface. The bending stiffness of a lipid monolayer is O(10 kT) (*4*), which would give it a wrinkle wavelength of O(1 μm) using $K = \rho g$. Wrinkles have been difficult to detect in lipids because of their poor scattering of light; however, diffuse x-ray scattering has shown wrinkle signatures with wavelengths of O(1 μm) (*4*, *26*). If the monolayer transforms as an elastic sheet, then we expect folds of the same order as the wavelength appearing perpendicular to the direction of compression; in particular, our scaling shows $l \sim \lambda^2/\Delta$, yet as the fold makes self-contact $\Delta \sim \lambda$, so $l \sim \lambda$. The most detailed study of monolayer folding where thousands of folding events were analyzed showed that the most probable folds in a model lung surfactant system were 2 μm in size and oriented

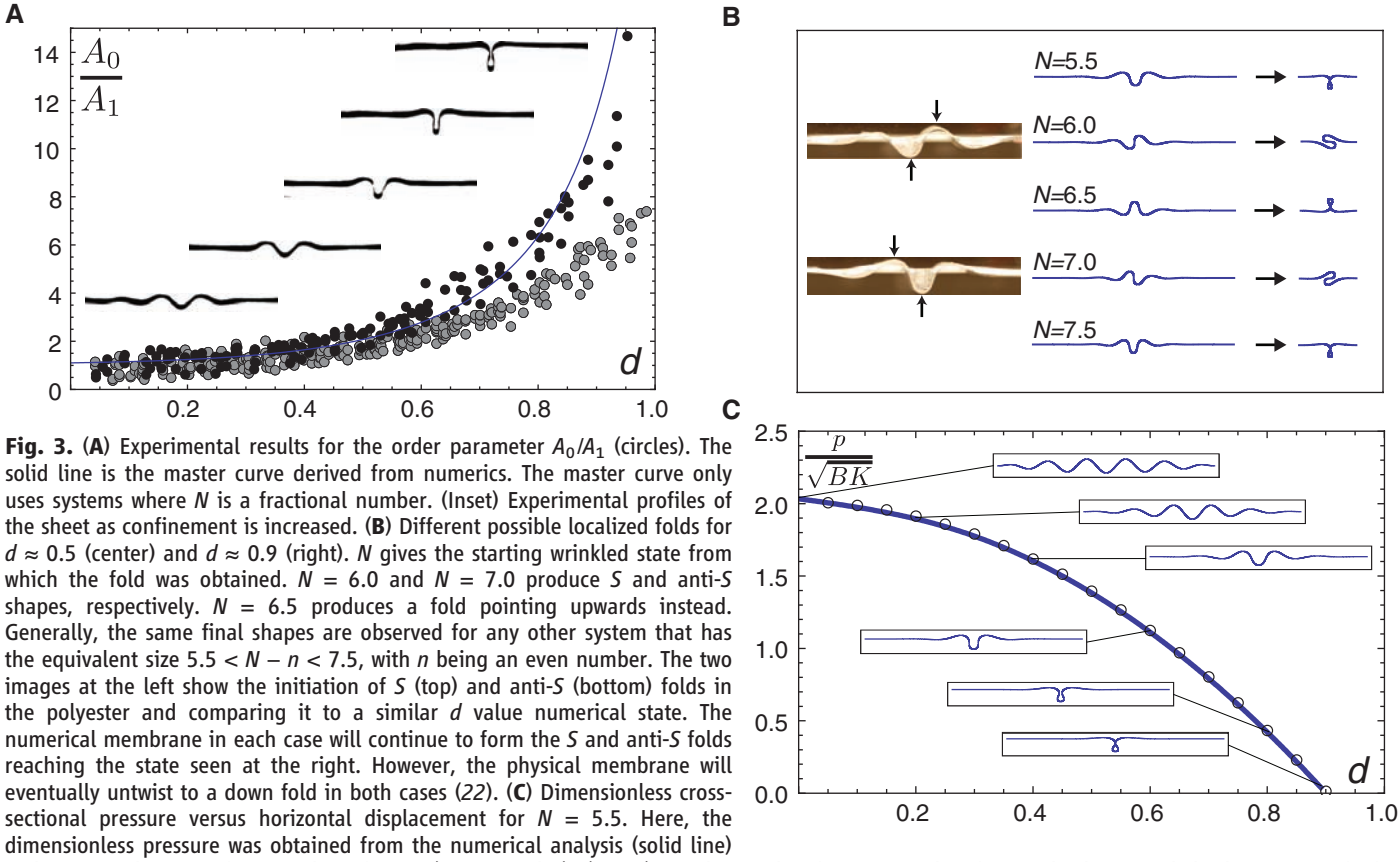

Fig. 3. (**A**) Experimental results for the order parameter A_0/A_1 (circles). The solid line is the master curve derived from numerics. The master curve only uses systems where N is a fractional number. (Inset) Experimental profiles of the sheet as confinement is increased. (**B**) Different possible localized folds for $d \approx 0.5$ (center) and $d \approx 0.9$ (right). N gives the starting wrinkled state from which the fold was obtained. $N = 6.0$ and $N = 7.0$ produce S and anti-S shapes, respectively. $N = 6.5$ produces a fold pointing upwards instead. Generally, the same final shapes are observed for any other system that has the equivalent size $5.5 < N - n < 7.5$, with n being an even number. The two images at the left show the initiation of S (top) and anti-S (bottom) folds in the polyester and comparing it to a similar d value numerical state. The numerical membrane in each case will continue to form the S and anti-S folds reaching the state seen at the right. However, the physical membrane will eventually untwist to a down fold in both cases (*22*). (**C**) Dimensionless cross-sectional pressure versus horizontal displacement for $N = 5.5$. Here, the dimensionless pressure was obtained from the numerical analysis (solid line) and compared to our theoretical prediction (empty circles). (Insets) Profiles of the sheet for each value of the horizontal displacement with the maximum amplitude normalized to 1.

directly perpendicular to the axis of compression (*28*). This is in agreement with our prediction. In the gold nanoparticle layers shown in Fig. 1C, wrinkles are more easily seen because of the strong scattering of the metal cores. As the image shows, the length scale over which the fold forms (*l*) is set by the initial wrinkle wavelength (λ).

Understanding compaction of nanometer-thin membranes through controllable and reversible modes like wrinkling and folding opens the door to technological use of these systems (*29*). In medicine, developing synthetic lung surfactant formulations depends on our capability to reproduce the incredible ability of native lung surfactant to compact by folding (*9*). Likewise, nanoparticle thin film applications rely on understanding the mechanical properties and responses of such layers (*12*, *13*, *29*). From wrinkle wavelengths, constants like the bending modulus can be found (*5*, *6*, *30*), whereas controlling the wrinkle-to-fold transition can help the development of adaptive functions in new technologies like flexible electronics (*29*, *31*).

References and Notes

1. T. A. Witten, *Rev. Mod. Phys.* **79**, 643 (2007).
2. A. Lobkovsky, S. Gentges, H. Li, D. Morse, T. A. Witten, *Science* **270**, 1482 (1995).
3. D. Vella, P. Aussillous, L. Mahadevan, *Europhys. Lett.* **68**, 212 (2004).
4. L. Bourdieu, J. Daillant, D. Chatenay, A. Braslau, D. Colson, *Phys. Rev. Lett.* **72**, 1502 (1994).
5. J. Huang *et al.*, *Science* **317**, 650 (2007).
6. N. Bowden, S. Brittain, A. G. Evans, J. W. Hutchinson, G. M. Whitesides, *Nature* **393**, 146 (1998).
7. R. Huang, Z. Suo, *J. Appl. Phys.* **91**, 1135 (2002).
8. H. Diamant, T. A. Witten, C. Ege, A. Gopal, K. Y. C. Lee, *Phys. Rev. E* **63**, 061602 (2001).
9. J. A. Zasadzinski, J. Ding, H. E. Warriner, F. Bringezu, A. J. Waring, *Curr. Opin. Colloid Interface Sci.* **6**, 506 (2001).
10. A. Gopal, K. Y. C. Lee, *J. Phys. Chem. B* **105**, 10348 (2001).
11. C. P. Collier, T. Vossmeyer, J. R. Heath, *Annu. Rev. Phys. Chem.* **49**, 371 (1998).
12. D. G. Schultz *et al.*, *J. Phys. Chem. B* **110**, 24522 (2006).
13. K. E. Mueggenburg, X. M. Lin, R. H. Goldsmith, H. M. Jaeger, *Nat. Mater.* **6**, 656 (2007).
14. S. T. Milner, J. F. Joanny, P. Pincus, *Europhys. Lett.* **9**, 495 (1989).
15. A. Saint-Jalmes, F. Graner, F. Gallet, B. Houchmandzadeh, *Europhys. Lett.* **28**, 565 (1994).
16. Q. Zhang, T. A. Witten, *Phys. Rev. E* **76**, 041608 (2007).
17. E. S. Nikomarov, *Langmuir* **6**, 410 (1990).
18. W. Lu *et al.*, *Phys. Rev. Lett.* **89**, 146107 (2002).
19. E. Cerda, L. Mahadevan, *Phys. Rev. Lett.* **90**, 074302 (2003).
20. Supporting material is available on *Science* Online.
21. H. Hertz, *Wiedemann's Ann. Phys. Chem. (Kyoto)* **22**, 449 (1884).
22. Although both up and down folds are observed, we note that the down fold is favored over the up fold. This asymmetry is not present in the numerics and can be accounted for by considering the meniscus geometry at the polyester/water/air contact line. Given that the wetting angle at the contact line is constant, the meniscus on the up fold will be slightly larger than the down fold. This geometric difference generates a slight asymmetry in the gravitational energy for the two states and favors the down fold. However, our current work has been done in a "deep" water regime. The up fold is more likely to be observed when the subphase is very shallow because the down fold cannot develop.
23. In certain conditions, a stretched state could play the role of a wrinkled state. The specific energy (U/L) for both has a finite value independent of system size. On the other hand, the specific energy of a folded state for a given applied strain Δ/L diverges to negative values for large systems. This predicts that a direct transition from a stretched to a folded state could be possible for large systems. The external compression necessary to observe a transition from a stretched flat surface to a wrinkled state is $\Delta_0 = L \times 2(BK)^{1/2}/Et$, where t is film thickness. The critical compression for the wrinkle to fold transition is $\Delta_1 = \lambda/3$. So a wrinkled state should be observed before folding if the inequality $\Delta_0 < \Delta_1$ or $L/\lambda < [3/(8\pi^2)](\lambda/t)^2$ is satisfied.
24. K. Efimenko *et al.*, *Nat. Mater.* **4**, 293 (2005).
25. H. E. Ries, W. A. Kimball, *J. Phys. Chem.* **59**, 94 (1955).
26. C. Ybert, W. Lu, G. Moller, C. M. Knobler, *J. Phys. Condens. Matter* **14**, 4753 (2002).
27. Solid monolayers continue to have positive surface tensions measured by Wilhelmy plates when they fold (*8*, *10*). Whereas the Wilhelmy plate accurately measures all interfacial forces at liquid interfaces, the measurement breaks down when the interface becomes solidlike (*32*). For a solid monolayer capable of supporting a deviatoric shear stress, a small increase in pressure at the periphery should lead to a smaller increase at the plate, with the weakening being governed by the ratio of shear to bulk moduli of the monolayer. Thus, parts of the monolayer close to the barriers may be under a compressive stress even if a finite surface tension is measured at the plate.
28. A. Gopal, V. A. Belyi, H. Diamant, T. A. Witten, K. Y. C. Lee, *J. Phys. Chem. B* **110**, 10220 (2006).
29. R. Vaia, J. Baur, *Science* **319**, 420 (2008).
30. The wrinkle wavelength observed in our experiments gives $B \sim 15$ kT for the gold layer. Using $B = Eh^3/12(1 - \nu^2)$, where t is the film thickness and ν is its Poisson ratio, we estimate the Young's modulus (E) of the 15-nm gold trilayer with $\nu = 0.3$ on the order of 100 kPa.
31. D.-H. Kim *et al.*, *Science* **320**, 507 (2008); published online 25 March 2008, 10.1126/science.1154367.
32. A. Saint-Jalmes, M. Assenheimer, F. Gallet, *J. Phys. Chem. B* **102**, 5810 (1998).

33. We thank T. Witten for many fruitful discussions as well as his leadership of the NSF Inter-American Materials Collaboration: Chicago-Chile (DMR-0303072) under whose support this collaboration began; M. Meron for many rich discussions; S. Rice, F. Melo, J. Pavez, A. Pocivavsek, and K. Lam for experimental help; and E. Sultan and A. Boudaoud for sharing their unpublished/in press manuscript "The Buckling of a Swollen Thin Gel Layer Bound to a Compliant Substrate" with us for guidance. This work was supported in part by the University of Chicago Materials Research Science and Engineering Center program of the NSF (DMR-0213745) and the U.S.-Israel Binational Foundation (2006076). L.P. thanks the University of Chicago Medical Scientist Training Program for support; A.K. was supported by the Dreyfus Summer Research Program at the University of Chicago (SG-06-039); K.Y.C.L. is grateful for support from March of Dimes (No. 6-FY07-357); R.D. and B.L. acknowledge the support of NSF/U.S. Department of Energy grant no. CHE-0535644 for ChemMatCARS; and E.C. acknowledges the support of Anillo Act 15, Fondap grant no. 11980002 and Fondecyt Project no. 1050083.

Supporting Online Material

www.sciencemag.org/cgi/content/full/320/5878/912/DC1
Materials and Methods
SOM Text
Fig. S1
Movies S1 and S2

12 December 2007; accepted 14 April 2008
10.1126/science.1154069

Metasomatized Lithosphere and the Origin of Alkaline Lavas

Sébastien Pilet,* Michael B. Baker, Edward M. Stolper

Recycled oceanic crust, with or without sediment, is often invoked as a source component of continental and oceanic alkaline magmas to account for their trace-element and isotopic characteristics. Alternatively, these features have been attributed to sources containing veined, metasomatized lithosphere. In melting experiments on natural amphibole-rich veins at 1.5 gigapascals, we found that partial melts of metasomatic veins can reproduce key major- and trace-element features of oceanic and continental alkaline magmas. Moreover, experiments with hornblendite plus lherzolite showed that reaction of melts of amphibole-rich veins with surrounding lherzolite can explain observed compositional trends from nephelinites to alkali olivine basalts. We conclude that melting of metasomatized lithosphere is a viable alternative to models of alkaline basalt formation by melting of recycled oceanic crust with or without sediment.

Trace-element and isotopic characteristics of alkaline [i.e., nepheline (ne)–normative] basalts from ocean islands and continents suggest the presence of enriched components in their mantle sources (*1*). These components are often interpreted as derived from recycled oceanic crust with or without sediment (*1*). An alternative is that the enriched components are recycled, metasomatized lithospheric mantle (*2*–*6*). Although both hypotheses are compatible with trace-element and isotopic characteristics of oceanic and continental alkaline magmas, they must also be capable of accounting for the distinctive major- and minor-element characteristics of alkaline basalts (Fig. 1).

Although basic to ultrabasic ne-normative liquids can be produced by low-degree melting of garnet lherzolite, no high-pressure melting experiments on "dry" peridotite have produced melt compositions that are plausible parents of alkaline ocean-island basalts (OIBs) (*7*–*10*). Addition of CO_2 to peridotite substantially modifies liquid compositions: Near-solidus melts are carbonatitic (*11*, *12*), but with increasing temperature, low-degree melts are silica-poor and CaO- and CO_2-rich (*11*). Such findings suggest that ne-normative magmas similar to natural alkaline basalts could be produced by low-degree melting (2 to 5%) of primitive mantle sources

Division of Geological and Planetary Sciences, California Institute of Technology, Pasadena, CA 91125, USA.

*To whom correspondence should be addressed. E-mail: sebastien.pilet@unil.ch